Journal of Magnetic Resonance **139,** 90–97 (1999)
Article ID jmre.1999.1772, available online at http://www.idealibrary.com on IDEAL®

A Novel High-Gradient Permanent Magnet for the Profiling of Planar Films and Coatings

P. M. Glover,[1] P. S. Aptaker,* J. R. Bowler, E. Ciampi, and P. J. McDonald

*Department of Physics, University of Surrey, Guildford, Surrey, GU2 5XH, United Kingdom; and *Resonance Instruments Ltd., Unit 13, Thorney Leys Business Park, Witney, Oxfordshire, OX8 7GE, United Kingdom*

Received September 25, 1998; revised January 20, 1999

The design and construction of a low-cost, permanent magnet is described. The magnet is intended for applications which require a large static gradient, such as those for which stray field imaging or fringe field diffusometry are conventionally employed. The magnet has been designed using the scalar potential method. Particular features of the magnet include a field profile such that $|\mathbf{B}|$ is constant in the horizontal plane and such that B is horizontal at the midpoint between the poles. There is a vertical, and therefore orthogonal, strong gradient, G, in $|\mathbf{B}|$. The ratio $G/|\mathbf{B}|$ is constant within a large volume and so allows measurements at a range of gradient strengths. It is this ratio which governs the shape of the pole-pieces. The constructed magnet has a typical operating field of 0.8 T, gives a gradient of 20 Tm^{-1}, and has a useable interpole access of 20 mm. Field plot data show values consistent with the theory. In particular $|\mathbf{B}|$ has a curvature of less than ± 5 μm over a 5 × 5 mm area at the target field. The magnet is most suitable for the one-dimensional profiling of thin planar samples. As an example of the magnet's use, a profile of a sandwich structure made of several polymer layers is shown. In addition, a set of one-dimensional profiles of an alkyd coating, recorded during solvent loss and cross-linking, is presented. This example demonstrates quantitative T_2 measurements at a resolution of 6.5 μm across a 70-μm-thick film.

Key Words: **magnet design; orthogonal gradient; stray field imaging; magnet pole-pieces; coatings.**

INTRODUCTION

Stray field imaging (STRAFI) and fringe field diffusometry methods (*1*) have become increasingly popular in recent times, with numerous applications found in the general areas of soft-solid and porous media analysis (*2*). Most commonly, the methods exploit the large on-axis field gradient located below a high-field superconducting vertical-bore NMR spectroscopy magnet. For example, our own 89-mm vertical-bore, 9.4-T magnet (Magnex Scientific Ltd., Abingdon, UK) has a gradient strength of the order of 58 Tm^{-1} at a field of 5.5 T some 20 cm below isocenter. While some applications undoubtedly require this high level of performance, there are many which do not, notably those involving semi-mobile systems with T_2 in the 100-μs to 1-ms range. In such cases, using a magnet with high homogeneity to generate an inhomogeneous field is not cost effective, and a low-cost alternative may be preferable.

There are other, geometry-related reasons why such a high-field magnet may not be the best system on which to carry out STRAFI experiments. Consider the drying, curing, and in-use efficacy of solvent-borne coatings systems (e.g., paints), the study of which is a common application area for STRAFI (*2*). These coatings start out as liquids and end up as solids and thus exhibit a wide range of T_2 values throughout the course of the experiment. STRAFI may be used to make one-dimensional T_2 profiles through the coating as a function of time with high spatial resolution. As the coating is initially liquid, the sample must be kept horizontal. However, the sample meniscus prevents the film from being entirely uniform across the sample area. In an earlier work, we introduced a probe for the profiling of the central uniform region of coating samples which overcame this constraint (*3*). However, although this probe proved highly successful, it was always evident that it was not the optimal solution.

In the conventional STRAFI arrangement illustrated in Fig. 1, the main field, $\mathbf{B}_0$, is oriented parallel to the gradient in the vertical direction. This arrangement necessitates, for a planar horizontal sample, an RF coil with the $\mathbf{B}_1$ field parallel to the sample plane. In order to localize the central region, we therefore used a small, horizontally oriented solenoid underneath the sample and accepted the consequent loss in sensitivity that this entailed. A much better arrangement, not available with conventional STRAFI, is to have the gradient in the vertical direction and $\mathbf{B}_0$ in the horizontal plane. Obtaining a profile is then possible with a planar-spiral surface-coil which has a vertical $\mathbf{B}_1$ field, as shown in Fig. 1. Locating the sample against the surface-coil offers improved sensitivity over conventional STRAFI as well as the desired transverse localization.

We therefore seek a low-cost, permanent magnet, having a horizontal magnetic field and a strong uniform linear field gradient in the vertical direction. Such a magnet permits the use of spin-echo Fourier transform methods to obtain profiles

[1] To whom correspondence should be addressed. Fax: +44 1483 876781. E-mail: p.glover@surrey.ac.uk.

1090-7807/99 $30.00

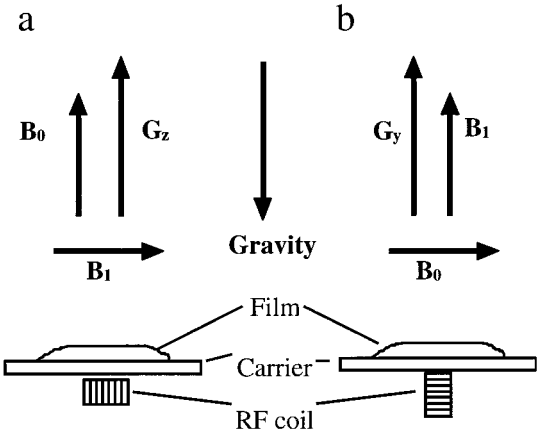

FIG. 1. Two possible geometrical configurations for stray field imaging: (a) the relative directions of static field, gradient, and RF for a conventional STRAFI system based on a vertical superconducting magnet; (b) the proposed magnet optimal geometry for thin-film imaging with the static field at right angles to the gradient.

of thin films and coatings. Similar magnets have been proposed previously for imaging applications. These include the so-called NMR MOUSE (*4*) and magnet designs by Miller and Garroway (*5*). However, with these magnets, no attempt is made to make the gradient homogeneous, as the main objective is for the analysis of a sample *outside* the confines of the magnet. Where there is slice selection, the slice is inevitably strongly curved. High-gradient magnets have also been designed for NMR diffusometry applications (*6*). These have field gradients of the order of 200 Tm^{-1} but are of no immediate relevance to the low-cost imaging applications envisaged here. The use of field gradients is not unique to NMR and they appear widely in other areas of science. Susceptibility measurement methods such as the Faraday method are based on the measurement of forces on a material suspended in an inhomogeneous field. Bending magnets for ion-beam accelerators also require tailored gradients and shaped pole-pieces. It is well known that a taper in the pole-pieces of a permanent or electromagnet will produce a field inhomogeneity or a gradient. This paper describes the calculation of the shape of magnet pole-pieces required to generate a magnetic field that is homogeneous over a plane, but possessing a powerful, orthogonal static gradient.

THEORY

For free space, Curl $\mathbf{B} = 0$ which leads to

$$G_y = \frac{\partial B_z}{\partial y} = \frac{\partial B_y}{\partial z}. \qquad [1]$$

With any spatially varying, static magnetic field there is an inevitable y-gradient in B_z (G_y) equal to the z-gradient in B_y. As a result of this, for the case where G_y is constant (a linear gradient), the equipotentials of $|\mathbf{B}|$ have a radius of curvature which is of the order of $|\mathbf{B}|/G_y$. For most conventional imaging (where $|\mathbf{B}|/G_y$ is of the order 10^2 m), this factor is not important, so it is possible to have near-linear gradients while transverse components of $\mathbf{B}$ are ignored. Generally, if a high gradient is required at a low-field strength, then the curvature of $|\mathbf{B}|$ cannot be ignored. There has been a succession of papers dealing with aspects of concomitant gradients in the areas of echo planar imaging (*7*); ESR (*8*); low-field diffusion measurements (*9*); and angiography corrections (*10*). In the case of STRAFI and the high-gradient strength profiling described here, it is the modulus of $\mathbf{B}$ that defines the plane of interest. For STRAFI with a conventional solenoidal electromagnet, there exists just one plane where $|\mathbf{B}|$ is uniform. It generally occurs at a slightly different position to the plane in which B_z is most uniform. The radius of field curvature is small (of the order of 0.1 m) and limits the achievable homogeneity of $|\mathbf{B}|$ in the plane and therefore the resolution. We seek to accommodate this difficulty with the new magnet.

It is proposed that the magnet pole geometry may be determined using a scalar potential approach where the potential, ϕ, is defined by $\mathbf{B} = \text{grad}\ \phi$. To a first approximation, there are no tangential components of $\mathbf{B}$ at the surface of a high-permeability, linear, and isotropic material, and therefore the material surface is also an equipotential surface. The shape of the pole-pieces is described by contours of a particular value of ϕ for an analytic solution to the Laplace equation, $\nabla^2\phi = 0$, which leads to the desired gradient and field values. In the analysis described here, the shape of the pole-pieces is assumed constant and infinite in the x direction. This assumption restricts the problem to two dimensions. The z-axis is defined as being the direction of the main, horizontal field, and the y-axis is the direction of the desired vertical gradient (see Fig. 1).

If ϕ is defined as a product of two independent polynomials, $Z(z)$ and $Y(y)$, which are both functions of a single axis coordinate, then

$$\phi(z, y) = Z(z)Y(y). \qquad [2]$$

Differentiating ϕ with respect to each axis gives the components of $\mathbf{B}$. Thus,

$$\mathbf{B} = \nabla\phi = \mathbf{j}Z(z)\frac{dY(y)}{dy} + \mathbf{k}\frac{dZ(z)}{dz}Y(y), \qquad [3]$$

where $\mathbf{j}$ and $\mathbf{k}$ are unit vectors in the y and z directions, respectively. As by definition $\nabla^2\phi = 0$, then

$$\frac{d^2Y(y)}{dy^2}\frac{1}{Y(y)} + \frac{d^2Z(z)}{dz^2}\frac{1}{Z(z)} = 0. \qquad [4]$$

Solutions of the set of simultaneous differential equations,

$$\begin{cases} \dfrac{d^2Y(y)}{dy^2} - A^2Y(y) = 0 \\ \dfrac{d^2Z(z)}{dz^2} + A^2Z(z) = 0 \end{cases}, \quad [5]$$

where A is a constant, may be found. The general form of the scalar potential that satisfies the above and that vanishes as $y \rightarrow \infty$ may be written as

$$\phi(z, y) = \exp(-Ay)(B\cos(Az) + C\sin(Az)), \quad [6]$$

where A, B, and C are real constants. If we choose the particular solution,

$$\phi(z, y) = a\sin(bz)\exp(-by), \quad [7]$$

where a and b are constants, then the components of $\mathbf{B}$ are given by

$$B_z = \frac{\partial\phi}{\partial z} = ab\cos(bz)\exp(-by) \quad [8]$$

and

$$B_y = \frac{\partial\phi}{\partial y} = -ab\sin(bz)\exp(-by). \quad [9]$$

The modulus of the field at any point is therefore

$$|\mathbf{B}| = ab\exp(-by). \quad [10]$$

Hence, the surface defined by a constant resonant frequency (constant $|\mathbf{B}|$) is a plane parallel to the x–z plane. Inevitably, the direction of $\mathbf{B}$ itself varies slightly across the plane of interest. As a result, when the magnet is used as described, $\mathbf{B}_1$ is not exactly orthogonal to $\mathbf{B}$ at the edge of the sample, and there is a small loss in sensitivity in this region (by the sine of a small angle). Apart from this, the field curvature is no problem.

We see from Eq. [10] that $|\mathbf{B}|$ is a function of y only. Differentiating $|\mathbf{B}|$ with respect to y yields the gradient G,

$$G = \frac{d|\mathbf{B}|}{dy} = -ab^2\exp(-by). \quad [11]$$

Over a small region of interest around $y = 0$, G can be deemed to be linear and equal to ab^2. The field $|\mathbf{B}|$ (at $y = 0$) is ab and therefore the $G/|\mathbf{B}|$ ratio is equal to $-b$. Equations [10] and [11] show that the $G/|\mathbf{B}|$ ratio is a constant, independent of both y and z. The implication of this fact is that, unlike conventional STRAFI based on a standard magnet, the user may choose to operate over a wide range of gradient values within the same magnet while maintaining the in-plane uniformity of the magnetic field.

The coordinates of the shape of the pole-pieces can be calculated from a particular equipotential of ϕ. The profile of the pole-pieces as a function of y-position is given as

$$z(y) = \pm\frac{\sin^{-1}(\sin(bw/2)\exp(by))}{b}, \quad [12]$$

where w is the pole separation at $y = 0$, and b is the desired $G/|\mathbf{B}|$ ratio. A family of curves may be obtained which vary from near-linear taper ($G/|\mathbf{B}| < 5\ \mathrm{m}^{-1}$) to a step function ($G/|\mathbf{B}| > 100\ \mathrm{m}^{-1}$). The latter is close to the NMR MOUSE design.

MATHEMATICAL MODELING

Equation [12] expresses what is considered to be the optimal analytic solution for the shape of the pole-pieces. It is dependent on b and w only. The actual values of $|\mathbf{B}|$ and a are determined by the magnetic materials used. The solution was initially verified in two dimensions and then in full three dimensions by utilizing electromagnetic finite element modeling tools (OPERA, Vector Fields, Oxford, UK). The magnet design targets were an operating field of 0.8 T and a $G/|\mathbf{B}|$ ratio of 25 m^{-1}, so as to give a gradient of 20 Tm^{-1}. The pole separation (w) at the target field was set to 20 mm. Figure 2 shows the shape of the pole-pieces viewed in cross section, as well as the location of the target plane, and Fig. 3 shows the three-dimensional wire-frame model of the magnet design. The pole-piece taper dimensions and angles below the throat, and also the pole-piece end taper (x-axis), were optimized to give the most economic use of magnetic materials without compromising the specification of the magnetic field. The throat gap was fixed at 11 mm so that a 10-mm sample tube could pass through. This design allows the mechanical movement of the sample, which is required for alternate imaging methods similar to those used in conventional STRAFI. Figure 4 shows the calculated $|\mathbf{B}|$ field along the vertical y-axis. The slightly exponential nature of the field can be seen. It is clear that across a sample of the order of a few hundred micrometers thick, the gradient can be assumed to be linear. The curvature is expressed as the maximum deviation of the numerically calculated $|\mathbf{B}|$ (finite element analysis) from the expected value (Eq. [10]) in a 5 × 5mm x–z plane. Converted to micrometers, this becomes

$$\text{curvature} = \frac{10^6(|\mathbf{B}_{\text{calc}}| - |\mathbf{B}_{\text{exp}}|)}{b}\ \text{in}\ \mu\text{m}. \quad [13]$$

This curvature is also shown in Fig. 4. It defines the vertical

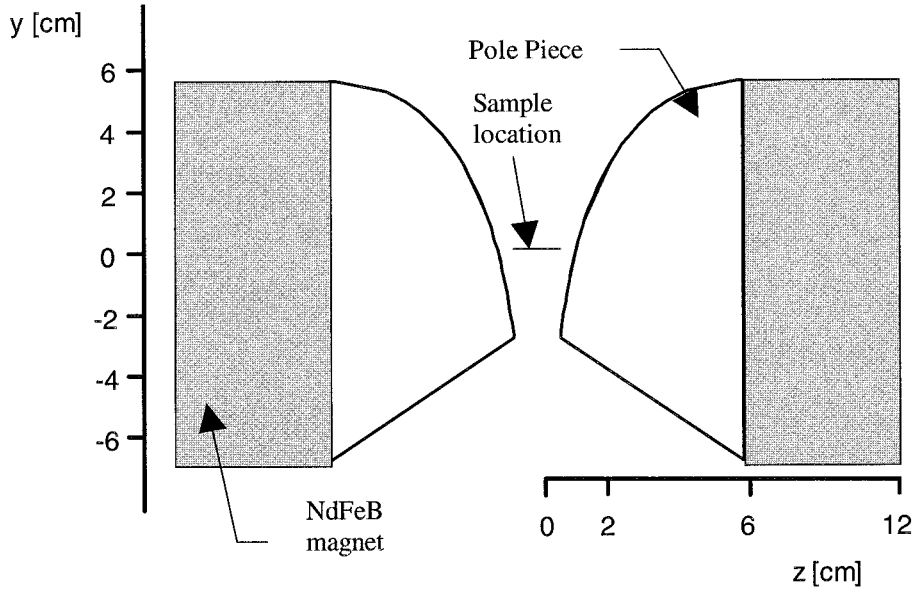

FIG. 2. Cross-section through the center of the magnet showing the shape of the pole-pieces, the lower taper, and the position of the sample.

extent to which any chosen plane is level and thus the useful imaging volume of the magnet. The sensitivities to both shear and interpole distance misalignment of the pole-pieces were calculated by finite element analysis. These were found to be vanishingly small even when the misalignments were set to extreme manufacturing tolerances. A single magnet based on this design can be used at any desired field strength between 0.5 and 1.0 T and, as $G/|\mathbf{B}|$ is constant, this gives gradients of between 12.5 and 25 Tm^{-1} while maintaining a field planar to better than 5 μm. A gradient of 20 Tm^{-1} allows resolution of a few micrometers without diffusion limits being reached for liquid-like samples (*4*).

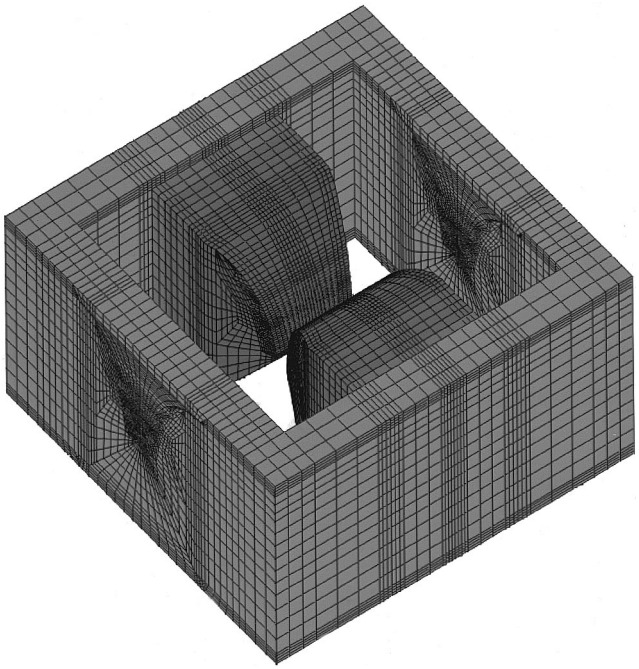

FIG. 3. Three-dimensional wire-frame model of the entire magnet, subsequently used in finite-element calculations, showing pole-pieces and taper of the *x*-axis. The total width of the magnet frame is 30 cm and the depth is 18 cm.

EXPERIMENTAL

The magnet was constructed using 5.7 kg of NdFeB for the magnet blocks and a 25-mm-thick iron frame. The Swedish steel pole-pieces were machined on a Bridgeport Portal 1500 three-axis numerically controlled milling machine. The performance of a five-axis machine, which would otherwise be required for such a complex shape, can be achieved on a three-axis mill by using a spherical cutting head. The pole-pieces were then annealed, chrome-plated, and assembled into the frame together with the magnet blocks.

The field profile of the magnet was initially verified using a three-axis, field-plotting rig and a Hall Probe Magnetometer (DTM-141 Digital Teslameter, Group 3, New Zealand), with 0.1-mT resolution and sensitive to B_z only. The magnet frame and Hall probe geometry did not permit the direct measurement of B_y. However, knowing the value and rate of change of B_z in both the x and y directions allows B_y (and hence $|\mathbf{B}|$) to be estimated by integrating Eq. [1], assuming that $B_y = 0$ T at $z = 0$ mm. In practice, a small misalignment between the magnet and the plot jig of 0.2 mm must be included as an integration constant, so $B_y = 0$ T at $z = 0.2$ mm. There is no measurable variation in B_z along the x-axis within the volume of interest, therefore $B_x = 0$ T. Figure 5 shows the measured

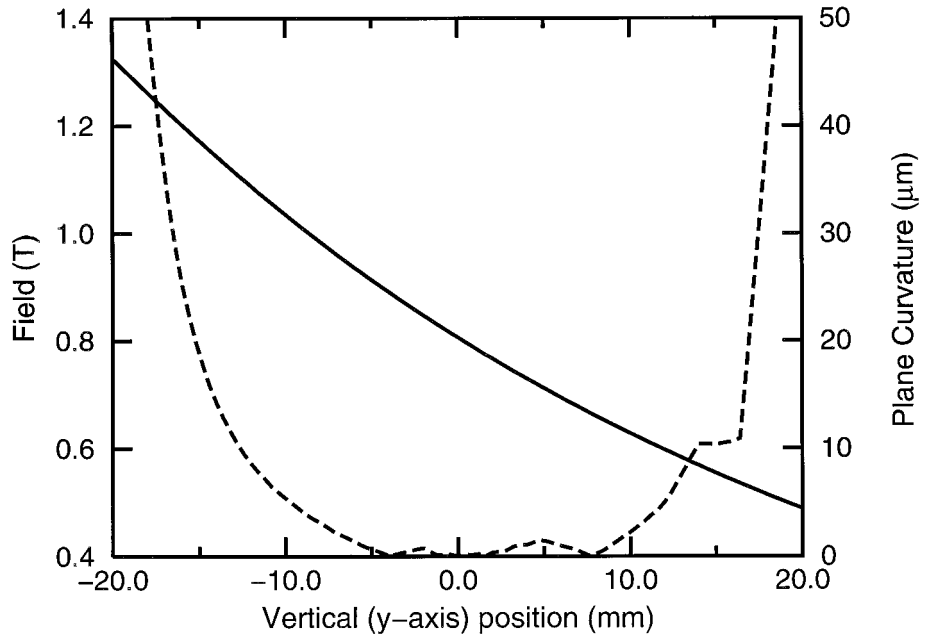

FIG. 4. Finite-element numerical simulations of the field strength (left axis, solid line), and the plane curvature (right axis, dashed line) against the magnet vertical y-axis position.

B_z, the estimated B_y, and the calculated $|\mathbf{B}|$ along the z-axis, i.e., between the poles for $x = 0$ mm and $y = 12$ mm. This measurement has been carried out at a slightly higher level than the target location (and hence at lower field) because the size of the Hall probe does not allow a full z-plane traversal any lower on the y-axis. The deviation from a uniform value of $|\mathbf{B}|$ is shown as an error in micrometers. The $|\mathbf{B}|$ is shown to be flat to better than ± 0.1 mT, equivalent to ± 5-μm error over the central 5-mm region of interest. This error is at the limit of the Hall probe specification and the positioning accuracy of the plotting rig but demonstrates that the target specification of the design has been achieved.

For NMR measurements, a precise leveling system is required to ensure that the sample carrier is parallel to the x–z

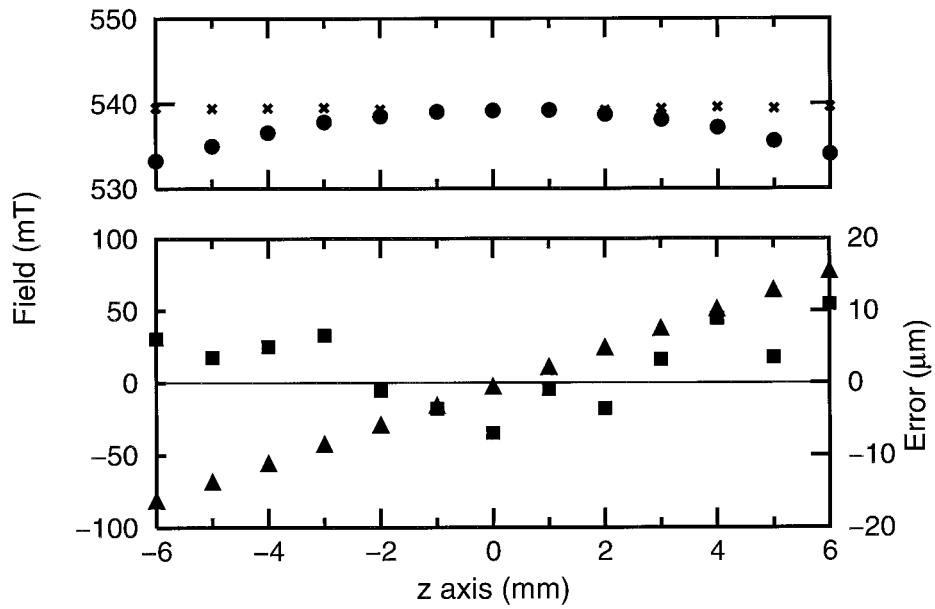

FIG. 5. Graph showing the field variation between the pole-pieces (z-axis) at a y position of 12 mm. The B_z values (circles) were measured using a Hall probe. The calculated values of B_y (triangles) and $|\mathbf{B}|$ (crosses) are shown along with the estimated error (squares, right axis).

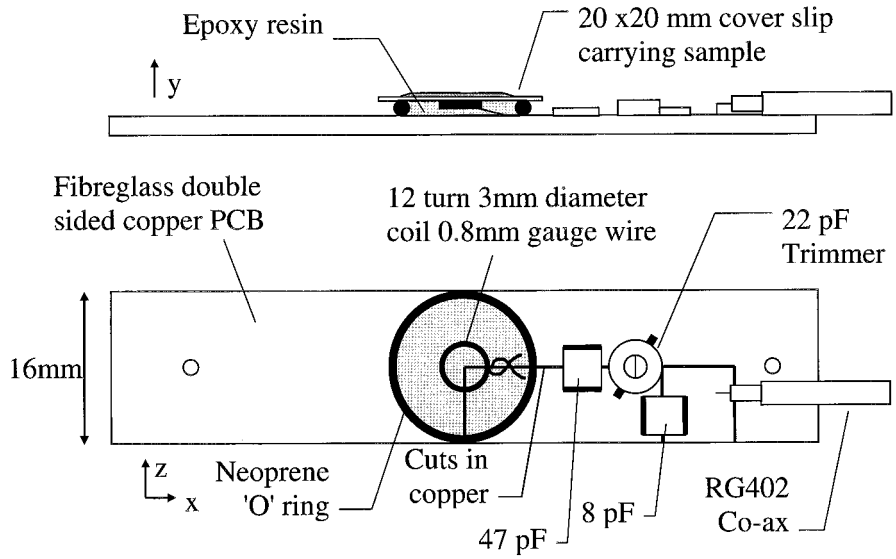

FIG. 6. Diagram of the RF probe in both elevation and plan view showing tuning and matching components. The probe mounts on a carrier that can be adjusted so that the sample is parallel to the x–z plane.

plane. This system comprises an "H" frame that is fixed by screw adjusters (at each corner of the H frame) to the magnet iron frame. The crossbar fits between the pole-pieces and supports the probe. The bar is interchangeable to accommodate different probes and a sample heating or cooling system. Minimizing the profile width of a phantom with parallel sides ensures that the sample is level. A suitable phantom is made using a room temperature vulcanizing silicone rubber film sandwiched between two glass coverslips, with spacers made from small pieces of 110-μm-thick coverslip. Using this method, the probe can be leveled to better than 10 μm over the planar region of interest (3 mm in diameter).

Figure 6 shows the design of a typical probe for use with the magnet. The design is similar to that of a microscope slide coil (*11*). The 3-mm-diameter coil comprises 12 turns of 0.8-mm-diameter polyurethane-coated wire arranged in three layers. The coil is supported in epoxy resin with the coil-end arranged to be flush with a flat upper surface. The probe (coil plus capacitors) has a resonant frequency of 30 MHz and a bandwidth of 1.0 MHz. The probe is located at the point where B = 0.7 T and the gradient is 17.5 Tm^{-1}. For ^{1}H measurements these parameters give an effective field of view along the vertical axis of the order of 700 μm. The pulse width required for a 90-degree flip angle is of the order of 1.0 μs at a power of 25 W. The sample area examined is approximately 3 mm in diameter. With samples less than 0.5 mm thick, the variation in flip angle and sensitivity is relatively small and is easily compensated.

RESULTS

A thin-layered phantom was fabricated from sheets of rubber, NESCO film, PVC tape, and polyamide tape attached to a 110-μm-thick glass coverslip. Figure 7 shows profiles of the phantom. An FID in the strong gradient is unobservable, as ring-down and dead-time effects last for 25 μs, of the order of T_2^*. Consequently, each profile is the Fourier transform of a separate echo in a β_x–[τ–β_y–τ–echo–]$_n$ sequence with τ = 75 μs. Due to the strong gradient and use of a surface coil, the

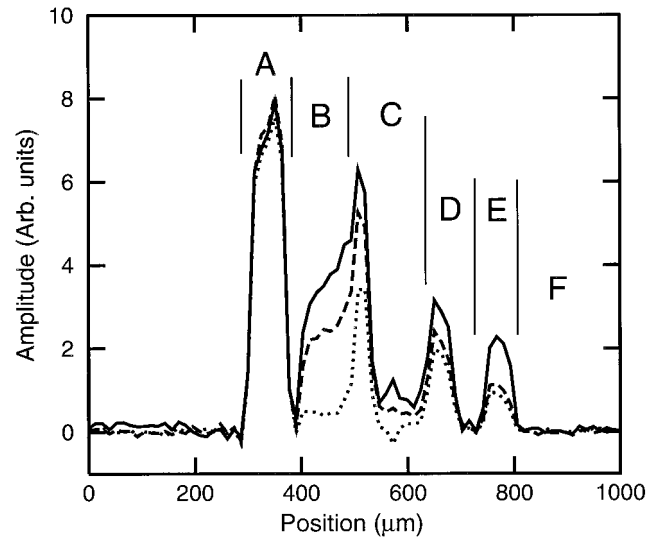

FIG. 7. Profiles of a thin-layer phantom made up of (A) rubber; (B) NESCO film; (C) PVC tape, and (D) polyamide tape. Also visible is a (E) polyamide tape layer that protects the RF coil. The RF coil location is designated by the symbol F. Each profile is the Fourier transform of a separate echo in a β_x–[τ–β_y–τ–echo–]$_n$ sequence where τ = 75 μs. For each echo, 256 points were acquired using a sampling interval of 0.4 μs, giving a pixel resolution of 13 μm. The solid line shows the first echo profile (multiplied by 1.5), the dashed line shows the second echo profile, and the dotted line shows the eighth echo profile from this sequence. Five thousand averages were acquired at a repetition time of 200 ms giving a total imaging time of 17 min.

pulse flip angle (β) is nominal, but of the order of 90° at the sample center. For each echo 256 data points were acquired at a sampling interval of 0.4 μs. The resulting profiles have a nominal pixel resolution of 13 μm. The profiles were acquired using 5000 averages and a repetition time of 200 ms, giving a total imaging time of 17 min. For this type of sequence, in the presence of a high gradient, the first echo is 2/3 the amplitude of the second echo (*2*), and this correction factor has been incorporated in the profiles of Fig. 7. Contrast resulting from the differences between long T_2 components, such as in the rubber and the glue on the back of the tapes, and short T_2 components, such as in the PVC and NESCO film, can be seen clearly. The glue backing of the polyamide tapes is also visible although the polyamide itself is not seen.

Figure 8 shows profiles of the same layered phantom but this time using a single asymmetric echo acquisition such that the effective primary echo time (TE) is reduced to 80 μs (compared to the TE = 150 μs of Fig. 7). The sampling interval was 0.4 μs, and 512 points were acquired to give a pixel resolution of 6.5 μm. The PVC and NESCO components of the profile have higher relative amplitudes compared to the rubber at the shorter echo time because they have much shorter T_2. In addition, a PMMA weight (placed on top of the glass coverslip to keep the phantom flat) (on left) and the epoxy around the RF coil (on right) are both now visible.

Profiles that demonstrate an application for which this type of magnet is particularly suitable are shown in Fig. 9. A low-molecular-weight alkyd with a cobalt catalyst additive was dissolved in a small quantity of solvent and spin-cast onto a coverslip to form a coating with a uniform thickness of around 120 μm. The coating on the coverslip was then placed on the probe in the magnet. Measurements were taken at half-hour intervals throughout the initial 3-h period and then at hourly intervals for a further 9 h. After 12 h the measurements were repeated daily. Quantitative T_2 values were obtained from single exponential fits to multiecho profiles using a β_x–[τ–β_y–τ–echo–]$_n$ sequence with τ = 150 μs and n = 8. These profiles have a resolution of 6.5 μm. During the first few hours there is some thinning of the film, presumably as a result of solvent evaporative loss. Subsequently, as the alkyd undergoes autooxidative cross-linking there is a reduction in T_2. There is evidence that the cross-linking is spatially nonuniform across the thickness of the film during this period. Eventually, however, the film becomes fully hardened and exhibits a more uniform T_2 profile. The process of hardening continues over a period of days and eventually results in a T_2 value of a few hundred microseconds for the whole alkyd film.

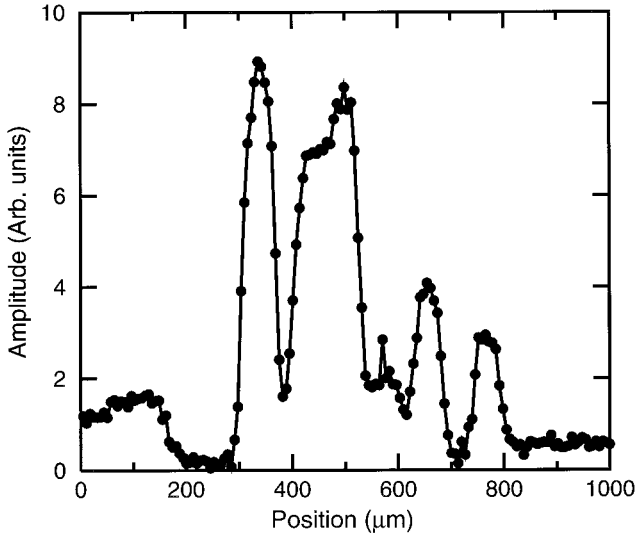

FIG. 8. A profile of the same phantom as in Fig. 7 but using a single-echo half *k*-space acquisition so that the effective echo time is reduced to 80 μs. Five hundred twelve points were acquired at a sampling interval of 0.4 μs giving an imaging resolution of 6.5 μm. A PMMA weight on top of a glass coverslip (on left) and the epoxy around the RF coil (on right) are now visible.

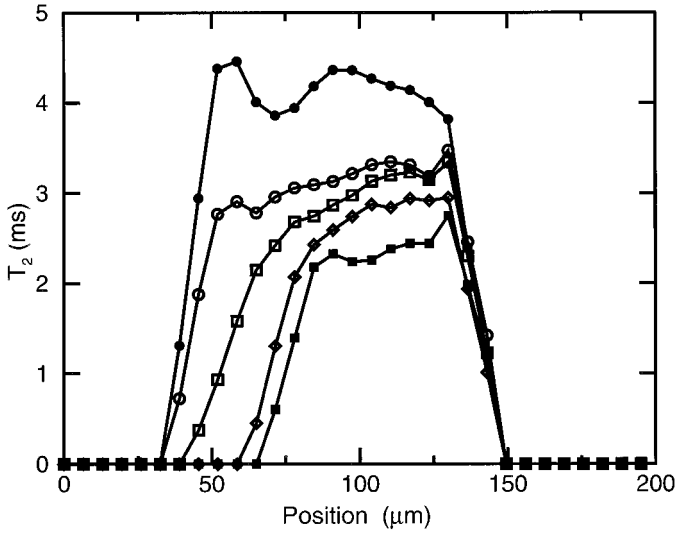

FIG. 9. T_2 profiles showing the solvent loss and cross-linking of an alkyd coating with cobalt catalyst and solvent. The filled circles indicate the profile of the film 0.5 h after spin-coating and at 1.5 h (open circles), 2.5 h (open squares), 1 day (diamonds), and 4 days (filled squares).

CONCLUSIONS

The scalar potential design method for a permanent magnet with a high ratio of orthogonal-gradient to main-field has been demonstrated. It is possible to generate a near-linear vertical gradient and homogeneous $|\mathbf{B}|$ in the horizontal plane over a large volume. The magnetic field within this volume has the property that the ratio $G/|\mathbf{B}|$ is constant. Therefore, the desired gradient, which scales with the static field, may be selected by appropriately positioning the sample and probe. $G/|\mathbf{B}|$ and the required pole separation determine the shape of the pole-pieces directly from an equipotential, and an exact analytic expression for this has been derived. No further modification to the shape of the pole-pieces was found to be required except for the optimization of the taper

of the lower and side edges. The design based on this analytic result has been shown to give the desired field by finite element numerical analysis, by experimental measurements with a Hall probe, and by MR measurements across suitable samples. Layered phantoms that demonstrate the planar $|\mathbf{B}|$, high-resolution imaging, and the ability to visualize short T_2 solids have been presented. Leveling of the sample has been achieved to around 10 μm across the sensitive region with simple profiling methods. A time-course study of both solvent loss and cross-linking of an alkyd coating (thickness of 120 μm) at 6.5-μm resolution has been presented as an example of a dynamic process that may be studied with the magnet. The geometry of the magnet is specifically optimized for the profiling of films. This design, coupled with its ease of access and use, makes this system applicable to a wide range of studies.

ACKNOWLEDGMENTS

We acknowledge the support of EPSRC and Unilever (Port Sunlight, UK) in funding this project. We also thank Robert Selway, Richard Hill, and Joseph Keddie for their assistance and valued contributions. We would also like to acknowledge ICI Paints (Slough, UK) for the donation of alkyd resins.

REFERENCES

1. A. A. Samoilenko, D. Yu. Artemov and A. L. Sibel'dina, Formation of sensitive layer in experiments on NMR subsurface imaging of solids, *JETP Lett.* **47,** 417–419 (1988).
2. P. J. McDonald, Stray field magnetic resonance imaging, *Prog. NMR Spectrosc.* **30,** 69–99 (1997).
3. P. M. Glover, P. J. McDonald, and B. Newling, Stray field imaging of planar films using a novel surface coil, *J. Magn. Reson.* **126,** 207–212 (1997).
4. G. Eidmann, R. Savelsburg, P. Blumler, and B. Blumich, The NMR MOUSE, a mobile universal surface explorer, *J. Magn. Reson. A* **122,** 104–109 (1996).
5. J. B. Miller and A. N. Garroway, US Patent 5 126 674 (1992).
6. I. Chang, F. Fujara, B. Geil, G. Hinze, H. Sillescu, and A. Tolle, New perspectives of NMR in ultra-high static magnetic field gradients, *J. Non-Cryst. Sol.* **172**(2), 674–681 (1994).
7. R. J. Coxon and P. Mansfield, EPI spatial distortion in non-transverse planes, Abstracts of the Society of Magnetic Resonance in Medicine, 8th Annual Meeting, Amsterdam, p. 1037 (1989).
8. D. G. Gillies, L. H. Sutcliffe, and M. R. Symms, Effects encountered in EPR spectroscopy and imaging at small magnetic-fields, *J. Chem. Soc. Faraday Trans.* **90**(18), 2671–2675 (1994).
9. J. Stepisnik, M. Kos, G. Planinsic, and V. Erzen, Strong nonuniform magnetic-field for self-diffusion measurement by NMR in the earth's magnetic-field, *J. Magn. Reson. A* **107**(2), 167–172 (1994).
10. M. A. Bernstein, X. H. J. Zhou, J. A. Polzin, K. F. King, A. Ganin, N. J. Pelc, and G. H. Glover, Concomitant gradient terms in phase contrast MR: Analysis and correction, *Magn. Reson. Med.* **39**(2), 300–308 (1998).
11. P. M. Glover, R. W. Bowtell, G. D. Brown, and P. Mansfield, A microscope slide probe for high resolution imaging at 11.7 Tesla, *Magn. Reson. Med.* **31,** 423–428 (1994).